Substitutional Electron and Hole Doping of WSe_{2}: Synthesis, Electrical Characterization, and Observation of Band-to-Band Tunneling

R. Mukherjee, H. J. Chuang, M. R. Koehler, N. Combs, A. Patchen, Z. X. Zhou, and D. Mandrus

Phys. Rev. Applied **7**, 034011 — Published 22 March 2017

DOI: 10.1103/PhysRevApplied.7.034011

Substitutional electron and hole doping of WSe_2: synthesis, electrical characterization, and observation of band-to-band tunneling

R. Mukherjee,[1] H. J. Chuang,[2] M.R. Koehler,[1] N. Combs,[1] A. Patchen,[3] Z. X. Zhou,[2] and D. Mandrus[1,4]

[1]*Department of Materials Science and Engineering, The University of Tennessee, Knoxville, TN 37996, USA*
[2]*Department of Physics and Astronomy, Wayne State University, Detroit, MI 48201, USA*
[3]*Department of Earth and Planetary Sciences, The University of Tennessee, Knoxville, TN 37996, USA*
[4]*Materials Science and Technology Division, Oak Ridge National Laboratory, Oak Ridge, TN 37831*

(Dated: February 23, 2017)

Transition metal dichalcogenides (TMDs) such as MoS_2, $MoSe_2$, and WSe_2 have emerged as promising two-dimensional semiconductors. Many anticipated applications of these materials require both p-type and n-type TMDs with long term doping stability. Here we report the synthesis of substitutionally doped WSe_2 crystals using Nb and Re as p- and n-type dopants, respectively. Hall coefficient and gate-dependent transport measurements reveal drastically different doping properties between nominally 0.5% Nb- and 0.5% Re-doped WSe_2. While 0.5% Nb-doped WSe_2 (WSe_2:Nb) is degenerately hole doped with a nearly temperature independent carrier density of $\sim 10^{19}$ cm^{-3}, electrons in 0.5% Re-doped WSe_2 (WSe_2:Re) are largely trapped in localized states below the mobility edge and exhibit thermally activated behavior. Charge transport in both WSe_2:Nb and WSe_2:Re is found to be limited by Coulomb scattering from ionized impurities. Furthermore, we have fabricated vertical van der Waals junction diodes consisting of multilayers of WSe_2:Nb and WSe_2:Re. Finally, we have demonstrated reverse rectifying behavior as a direct proof of band-to-band tunneling in our WSe_2:Nb/WSe_2:Re diodes.

I. INTRODUCTION

Transition metal dichalcogenides (TMDs) have demonstrated a number of two-dimensional semiconducting properties desirable for nanoelectronics, including a relatively high carrier mobility, mechanical flexibility, and chemical and thermal stability [1–3]. Moreover, TMDs offer the advantage of a substantial band gap essential for low power digital electronics [4–9] when compared to graphene. Similar to silicon-based electronics, controlled p- and n-type doping of TMDs with good air and thermal stability is essential for applications such as field-effect transistors (FETs) and $p-n$ junction diodes. Of particular note is that the underlying operation mechanism of $p-n$ junctions formed by the van der Waals assembly of heavily doped TMDs is expected to be quite different from conventional semiconductor $p-n$ junctions. While the current in a conventional semiconductor $p-n$ junction is limited by a bias-dependent depletion region, the bias voltage drop in a vertical TMD $p-n$ junction is expected to occur mostly across a van der Waals gap at the interface of the p- and n-type TMD semiconductors [10]. Consequently, the current under forward bias in a TMD $p-n$ junction is expected to be dominated by the tunneling-assisted recombination of the majority carriers through a van der Waals gap, as was recently observed in atomically thin TMD heterostructure $p-n$ junctions [11]. More interestingly, band-to-band-tunneling (BTBT) of electrons from the valence band of the p-type TMD to the conduction band of the n-type TMD can occur under reverse bias, which is the foundation of BTBT transistors.

Experimentally, $p-n$ junctions composed of p-type and n-type TMD semiconductors have demonstrated rectifying behavior similar to conventional $p-n$ junctions [10–15]. However, the reverse current in these devices has been largely limited by a lateral depletion region instead of a vertical p-n junction because the doping of at least one constituent TMD is inadequate [11, 14]. This lateral depletion barrier under reverse bias prevents the observation of BTBT. In order to reveal the intrinsic properties of TMD-based van der Waals $p-n$ junctions and achieve BTBT, it is necessary to heavily p- and n-dope the TMDs forming the $p-n$ junction.

From a technological point of view, doping directly into the valence or conduction bands is challenging but interesting. Various doping methods, such as surface transfer doping [6, 7, 16, 17] and chemical doping [14, 18], have been employed to control the type and density of majority carriers in TMDs. However, doping achieved using most of these methods lacks sufficient air, thermal or long-term stability. In this respect, substitutional doping achieved during crystal growth yields excellent air and thermal stability since dopants in this case are secured by covalent bonding [14].

While substitutional doping during the growth of TMD crystals has been reported previously [14, 19], only a handful of electrical transport studies have been reported [20, 21]. Among the most heavily studied TMDs (e.g., MoS_2, $MoSe_2$, WS_2 and WSe_2), WSe_2 has demonstrated the highest room-temperature intrinsic hole mobility (up to 500 cm^2 V^{-1} s^{-1}) [5]. Furthermore, WSe_2 is more resistant to oxidation in humid environments than the more extensively studied MoS_2 [8, 22].

In this paper, we report the synthesis and electrical characterization of heavily p- and n-doped WSe_2 crystals by substitutionally replacing 0.5% of W with Nb and 0.5% of W with Re. Resistivity and Hall-effect measurements were performed on bulk samples, and gate-dependent transport measurements were performed on mechanically exfoliated few-layer crystals. We find that

WSe_2:Nb is degenerately *p*-doped to a nearly temperature independent hole density of ~ 10^{19} cm^{-3} down to cryogenic temperatures. On the other hand, the electron density of WSe_2:Re determined by Hall effect measurement decreases exponentially from ~ 10^{17} cm^{-3} at room temperature to ~ 10^{15} cm^{-3} at 100 K. The observed differences in carrier density and temperature dependence indicate substantially different doping mechanisms between WSe_2:Nb and WSe_2:Re, which is consistent with theoretical modeling [23]. Both WSe_2:Nb and WSe_2:Re show similar Hall mobility values of ~ 5 cm^2 V^{-1} s^{-1} at room temperature. While the mobility of WSe_2:Nb is nearly temperature independent down to 100 K, that of WSe_2:Re decreases by 2–3 times as the temperature decreases from room temperature to 100 K. The relatively low mobility found in WSe_2:Nb and WSe_2:Re is primarily limited by ionized impurity scattering from dopant ions in the crystals. The difference in the temperature dependence of the Hall mobility between WSe_2:Nb and WSe_2:Re can be attributed to weakened screening of Coulomb potentials with decreasing carrier density. The field-effect mobility and carrier density estimated from the Drude model in multilayer WSe_2:Nb are in reasonably good agreement with the Hall effect measurement results on bulk samples. However, Hall effect and field-effect measurements yield drastically different carrier density and mobility values in WSe_2:Re. These discrepancies observed in WSe_2:Re can be attributed to the fact that the Hall effect and field-effect measurements probe different charge carriers. While Hall effect measurements probe only delocalized charge carriers above the mobility edge, the field-effect measurements include both free and trapped carriers [24]. In addition to the electrical transport measurements on the doped materials, we have also fabricated vertical *p*-*n* junctions by van der Waals assembly of Nb-doped and Re-doped WSe_2 multilayers and observed BTBT under reverse bias.

II. EXPERIMENT

WSe_2:Nb (0.5% nominal doping) and WSe_2:Re (0.5% nominal doping) crystals were grown using chemical vapor transport in sealed silica tubes from polycrystalline powders and iodine as a transport agent. The polycrystalline powders were prepared from stoichiometric mixtures of Nb (99.99%), Re (99.999%), W (99.999%) and Se (99.999%) and sealed in silica tubes under vacuum. The tubes were slowly heated to 900°C in order to prevent explosion due to excessive Se vapor pressure. The ampoules remained at 900°C for approximately 7 days and were allowed to furnace cool to room temperature. Phase purity was confirmed with powder X-ray diffraction. Single crystals of WSe_2 were then grown using the polycrystals as starting material and ~ 17.5 mg of iodine per cm^3 of tube volume. The silica tubes containing phase-pure powder and iodine were sealed under vacuum and placed in a tube furnace with a 50°C temperature gradient from the hotter end of the tube containing the charge (1050°C) to the colder end where growth occurs (1000°C). Crystals in the form of shiny silver plates with typical size $5 \times 5 \times 0.1$ mm^3 grew over the course of 5 days. Elemental analysis was performed using wavelength dispersive spectrometry (WDS) on a Camec SX 100 electron microprobe. An accelerating voltage of 20 kV and beam current of 40 nA were used in a spot size of 5 microns. $CaWO_4$, Re, CdSe and $SnBaNb_4O_{10}$ were used as standards for quantification. Detection limit of the spectrometer is around 0.03 wt.%. Quantitative analysis of $Nb_xW_{1-x}Se_2$ and $Re_xW_{1-x}Se_2$ revealed actual dopant concentration of x= 0.40 at.% and 0.42 at.% respectively.

To fabricate FETs, multilayer crystals of WSe_2:Nb and WSe_2:Re were produced by repeated splitting of corresponding bulk crystals using a mechanical cleavage method. The multilayer crystals were then transferred to a degenerately doped Si substrate with a 270 nm SiO_2 layer. Optical microscopy was used to identify thin WSe_2:Nb and WSe_2:Re crystals, which were further characterized by a Park-Systems XE-70 non-contact atomic force microscope (AFM). Drain and source electrodes were subsequently fabricated using standard electron beam lithography and electron beam deposition of 5 nm Ti and 40 nm Au. The degenerately doped Si substrate was used as a back gate for the fabricated FETs.

BTBT based heterojunction diodes were fabricated by van der Waals assembly of multilayered WSe_2:Nb and WSe_2:Re flakes, as shown in the top inset of Fig. 3(a). First, Au/Ti (30 nm/10 nm) bottom electrodes were fabricated on a SiO_2/Si substrate. WSe_2:Nb thin flakes (red in Fig. 3(a)) were then prepared on a clean polydimethylsiloxane (PDMS) stamp and transferred onto the top of the electrodes as the *p*-side of the diode; subsequently, WSe_2:Re flakes (green in Fig. 3(a)) were transferred and stacked on top of the WSe_2:Nb flakes as the *n*-side. Finally, Au/Ti top electrodes were fabricated on the WSe_2:Re flakes to complete the fabrication of the vertical *p*-*n* junction device.

Temperature and magnetic field-dependent Hall effect and resistivity measurements were carried out in a Quantum Design Physical Property Measurement System. Resistivity and Hall measurements were carried out on bar shaped crystals of dimension $5 \times 1.5 \times 0.2$ mm^3. High purity silver paste from SPI Supplies and 25 μm diameter gold wires were used for electrical contacts. Hall measurements were made from 4–300 K in applied magnetic fields up to 5 Tesla.

III. RESULTS

A. Resistivity and Hall measurements on bulk

Fig. 1(a) shows the resistivity measured in the basal plane from 10–300 K for WSe_2:Nb and from 50–300 K for WSe_2:Re. The resistivity (ρ) of WSe_2:Nb is found to be ~ 10^{-2} Ω cm and nearly temperature independent. The

resistivity of WSe_2:Re is over two orders of magnitude higher than WSe_2:Nb at room temperature and increases by five orders of magnitude as the temperature decreases to ~50 K. To shed light on the drastically different electrical properties of Nb- and Re-doped WSe_2, we performed Hall effect measurements to determine the carrier density and mobility. The Hall resistivity (ρ_{xy}) is derived from the Hall voltage as follows:

$$\rho_{xy} = V_H/I_x = R_H B_z/t \quad (1)$$

where V_H is the Hall voltage, R_H is the Hall coefficient, I_x is the longitudinal current, B_z is the magnetic field perpendicular to the sample, and t is the thickness of the sample. The Hall coefficient R_H is determined from the slope of the linear fit of the Hall resistivity as a function of magnetic field (H) as shown in Fig. 1(b). In a simple one-band model, the sign of R_H determines if the carriers are electrons or holes, and the carrier density is given by $n = 1/|R_H|e$, where n is the carrier density and e is the charge of the electron.

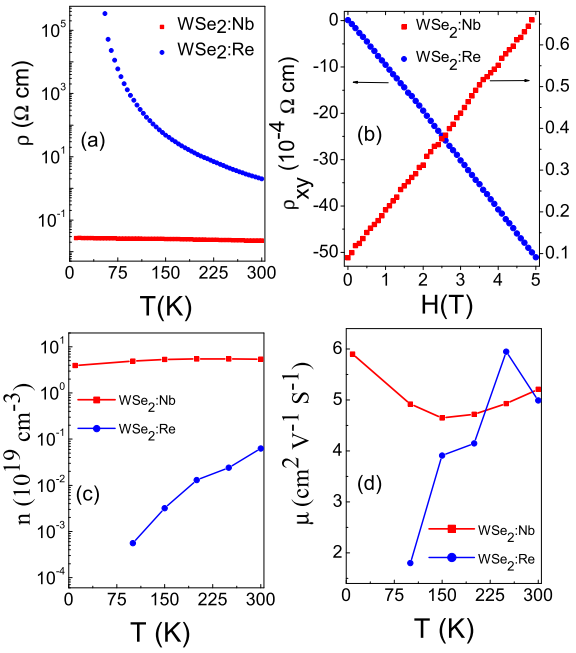

FIG. 1. (a) Resistivity as a function of temperature for WSe_2:Nb (red squares) and WSe_2:Re (blue circles). (b) Linear behavior of Hall resistivity as a function of magnetic field at 300K is shown. The positive slope for WSe_2:Nb and negative slope for WSe_2:Re confirms p-type and n-type, respectively. (c) Inferred carrier density vs. temperature for Nb- and Re-doped WSe_2. Freezing of charge carriers is not observed in WSe_2:Nb, whereas the carrier concentration decreases with temperature for WSe_2:Re. (d) Hall mobility vs. temperature for Nb- and Re-doped WSe_2. A weak dependence on temperature is clearly seen for WSe_2:Nb, whereas the mobility decreases by roughly a factor of three for WSe_2:Re as the sample is cooled

Fig. 1(c) shows the carrier density of Nb- and Re-doped WSe_2 as a function of temperature. The hole density of WSe_2:Nb at room temperature is approximately 5.2×10^{19} cm^{-3} and the electron density of WSe_2:Re at room temperature is approximately 6.3×10^{17} cm^{-3}. Now, following the WDS analysis if we assume one hole per niobium atom, then the maximum hole concentration that could possibly exist in a crystal is 6.5×10^{19} cm^{-3} which agrees reasonably well with the Hall measurement. Interestingly, the hole density in WSe_2:Nb remains nearly constant for the entire measured temperature range (10–300 K), while the electron density in WSe_2:Re decreases by about two orders of magnitude as the temperature decreases from 300 to 100 K. Apparently, the charge carriers in WSe_2:Nb do not freeze out even at cryogenic temperatures, which is a strong indication of degenerate doping. This also suggests that the acceptor states introduced by the Nb dopants are close to the valence band maximum and are highly delocalized. On the other hand, the electron density in WSe_2:Re shows thermally activated behavior. An activation energy of ~ 60 meV can be inferred by plotting carrier density as a function of 1/T on a semi-log scale (not shown here), suggesting that localized donor impurity states are formed ~ 60 meV below the conduction band minimum. Our results are in good agreement with a recent theoretical calculation of Nb and Re doping of TMDs [23].

In addition, we have also calculated the Hall mobility (μ_H) from the measured resistivity and carrier density using the equation $\mu_H = R_H/\rho_{xx}$. Fig. 1(d) shows the Hall mobility of WSe_2:Nb and WSe_2:Re as a function of temperature. The mobility values of Nb- and Re-doped WSe_2 are both around 5 cm^2 V^{-1} s^{-1} at room temperature, but they show different temperature dependencies. The Hall mobility of WSe_2:Nb is nearly temperature independent down to cryogenic temperatures. On the other hand, the Hall mobility of WSe_2:Re decreases by a factor of 3 as the temperature decreases from 300 K to 80 K. These characteristics of doped WSe_2 are found to be different than undoped WSe_2 whose Hall mobility is around 60 cm^2 V^{-1} s^{-1} with carrier density ~ 10^{16} cm^{-3} at room temperature. The relatively low mobility values in comparison with undoped WSe_2 may be attributed to increased ionized impurity scattering due to the presence of Nb and Re ions [25–27]. The contrast in temperature dependence of the Hall mobility in Nb- and Re-doped WSe_2 can be explained by free-carrier screening of the Coulomb potential of the ionized impurities. The decrease of electron density with decreasing temperature in WSe_2:Re reduces the charge screening of Coulomb potential of the ionized impurities, leading to reduced electron mobility at lower temperatures. On the other hand, hole density in WSe_2:Nb does not vary with temperature; consequently, the Coulomb scattering in WSe_2:Nb is also temperature independent.

B. Charge transport in multi-layered flakes of Nb- and Re-doped WSe_2

To shed additional light on the transport mechanisms in Nb- and Re-doped WSe_2, we have also measured electric field tuned conduction in FETs fabricated from multilayer WSe_2:Nb and WSe_2:Re. We chose to focus on multilayered FETs as they allow higher drive currents and are less affected by the substrate in comparison with monolayer devices. The fabricated devices were electrically characterized at room temperature under different drain and gate voltages, as shown in Fig. 2. An atomic force microscopy (AFM) image of a typical WSe_2:Nb FET is shown in the Fig. 2(a) inset. Fig. 2(a) and (b) show drain

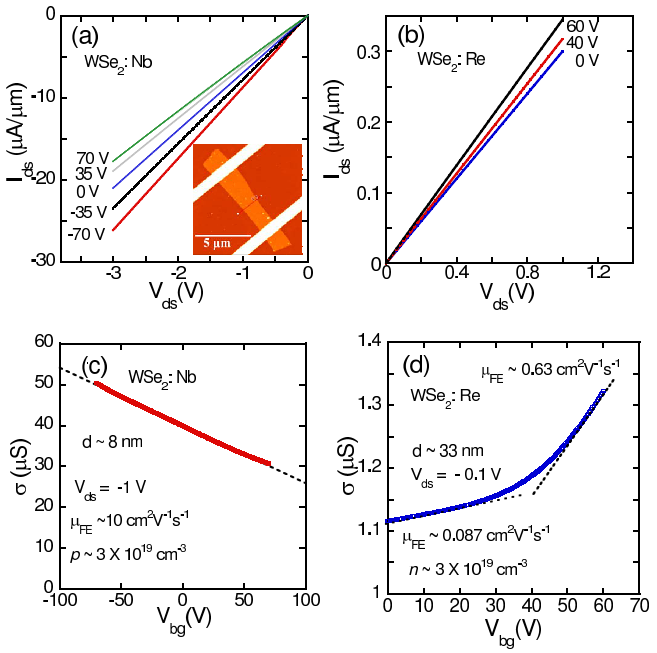

FIG. 2. Linear behavior of drain current as a function of drain-source voltage for different gate voltages are shown for (a) Nb-doped WSe_2 and (b) Re-doped WSe_2. The inset in Fig. (a) shows AFM image of WSe_2:Nb FET. (c) Shows the dependence of conductivity on back gate voltage for hole-doped WSe_2:Nb when drain voltage is -1 V and (d) shows dependence of conductivity for electron-doped WSe_2:Re when drain voltage is -0.1 V.

current (I_{ds}) as a function of drain-source voltage (V_{ds}) at several different gate voltages for two representative FETs consisting of 8 nm thick WSe_2:Nb and 33 nm thick WSe_2:Re, respectively. The linear behavior of I–V characteristics at all gate voltages suggests the formation of Ohmic contacts, which is attributed to narrow Schottky barriers due to the large carrier concentration in doped WSe_2. It should also be noted that there is a small increase of I_{ds} as the gate voltage changes from 70 V to -70 V for WSe_2:Nb and 0 V to 60 V for WSe_2:Re, indicating heavy p- and n-type doping, respectively. Fig. 2(c) and (d) show the two-terminal conductivity of WSe_2:Nb and WSe_2:Re as a function of back gate voltage (V_{bg}). The conductivity is defined as $\sigma = (I_{ds}/V_{ds}) \times L/W$, where L and W are the length and width of the channel, respectively. The field-effect mobility (μ_{FE}) is extracted from the conductivity as a function of gate voltage using the expression $\mu_{FE} = (1/C_{bg}) \times (d\sigma/dV_{bg})$, where C_{bg} is the back-gate capacitance per unit area. Based on a simple parallel plate capacitor model, C_{bg} is determined to be 1.3×10^{-8} F cm^{-2} for 270 nm SiO_2 ($C_{bg} = 3.9\times\epsilon_0/270$ nm). The slope of the linear fit shown in Fig. 2(c) gives $\mu_{FE} \sim 10\ cm^2\ V^{-1}\ s^{-1}$ for WSe_2:Nb, which agrees reasonably well with the Hall mobility (μ_H). μ_{FE} for WSe_2:Re, however, is found to be 0.087 cm^2 V^{-1} s^{-1} at low gate voltages and increases to 0.63 cm^2 V^{-1} s^{-1} at high gate voltages, which is one to two orders of magnitude lower with respect to the corresponding Hall mobility (μ_H).

The discrepancy between the Hall mobility and field-effect mobility in WSe_2:Re can be attributed to the fact that charge density measured by these two methods can be different depending on the nature of the charged carriers. In the field-effect measurement, the charge density is estimated from $Q = C_{bg}(V_{bg} - V_{th})$, where V_{th} is the threshold voltage. Here, the charge density Q includes both trapped charges occupying localized states below the mobility edge (Q_{loc}) and free carriers thermally excited to the delocalized states above the mobility edges (Q_{free}). On the other hand, the carrier density obtained from the Hall measurement includes only the free carriers above the mobility edge. Since only a small fraction of the total carrier density in WSe_2:Re is thermally excited into delocalized states above the mobility edge and the mobility of free carriers is much larger than that of the localized carriers, the field-effect mobility (μ_{FE}) calculated from $\Delta\sigma/\Delta Q$ is expected to be much smaller than the Hall mobility calculated from σ/Q_{free} [28]. Furthermore, more free carriers are excited to the delocalized states above the mobility edge as the chemical potential moves up with increasing gate voltage, leading to the increase of field-effect mobility as shown in Fig. 2(d). In contrast, nearly all carriers in WSe_2:Nb are free, which leads to similar values for the Hall mobility and field-effect mobility because the majority of the carriers in WSe_2:Nb are delocalized and contribute to the conductivity. The slightly larger value of field-effect mobility in comparison with the Hall mobility can be explained by the increase of mobility with increasing carrier density at higher negative gate voltages. As a result, the field-effect mobility overestimates the mobility by $\mu_{FE} = \mu_H + n(d\mu_H)/(C_{bg}dV_{bg})$ [29]. These results are also in good agreement with the theory that Nb-doping forms delocalized states that overlap with the valence band, and Re-doping introduces localized states below the conduction band of TMDs [23]. We also extracted the carrier density (n) from the conductivity at zero gate voltage and the field effect mobility using the Drude model: $\sigma = ne\mu$. The charge density at room temperature for the thin flake sample of WSe_2:Nb in Fig. 2 is $\sim 3\times10^{19}$ cm^{-3}, which agrees with the carrier density from the Hall measurement whereas the charge density of the WSe_2:Re thin flake at zero gate voltage is $\sim 3\times10^{19}$ cm^{-3}, which is two orders of magnitude higher than that

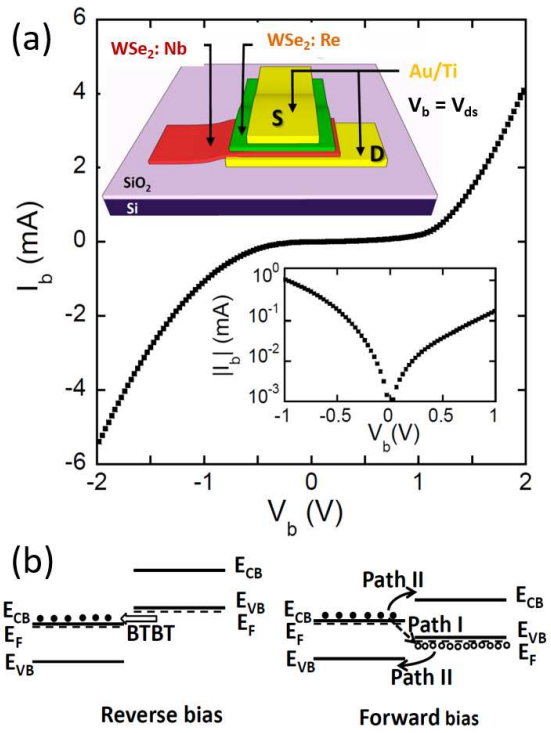

FIG. 3. (a) Current as a function of applied bias V_b on Si while WSe_2:Re is grounded. The *p*-*n* junction characteristics are shown in both forward and reverse bias conditions. The upper inset shows the schematic diagram of the hetero-junction device, and the lower inset shows the order of rectification from forward to reverse bias of 2 V. (b) Qualitative band diagrams at forward and reverse biases. BTBT tunneling is shown in reverse bias and the hole/electron recombination process is shown in forward bias.

found from Hall measurement but similar to the hole density in WSe_2:Nb. The higher carrier density extracted from the field-effect measurement can be attributed to the electrons trapped in localized states that cannot be detected by Hall effect measurement. Significantly higher Re concentration or different *n*-dopants may be needed to synthesize degenerately *n*-doped WSe_2 and other TMDs.

C. Demonstration of band to band tunneling

Another advantage of two dimensional transition metal dichalcogenides is that they can be promising materials for developing BTBT transistors, which enable steeper subthreshold swing and the down scaling of the supply voltage beyond the fundamental thermionic limit [30, 31]. As a significant step toward this direction, we have experimentally demonstrated the operation of a backward diode in a WSe_2:Nb/WSe_2:Re vertical heterojunction as schematically shown in the top inset of Fig. 3(a). A bias voltage (V_b) is applied on WSe_2:Nb (terminal "d") and WSe_2:Re (terminal "s") is grounded. Fig. 3(a) shows the I_b–V_b characteristics of the device. Drastically different from the behavior of conventional *p*-*n* junction diodes, the reverse current in our van der Waals assembled *p*-*n* junction is larger than the forward current at relatively low bias voltages ($|V_b| < 1$ V), as shown in the lower inset of Fig. 3(a). The reverse rectifying behavior observed here provides strong evidence of electron tunneling from the valence band of *p*-type WSe_2:Nb to the conduction band of WSe_2:Re.

Note that the operation mechanism of vertical van der Waals assembled diodes differs fundamentally from that of conventional *p*-*n* diode devices. In the latter case, the flow of electrons or holes is hindered by the built-in potential that gives rise to a depletion region at the *p*-*n* junction. In the TMD BTBT device, no such depletion region is necessary because potential can be dropped across the thin van der Waals gap at the *p*-*n* interface, which allows the bands of the two material components to move freely with respect to one another under an applied bias voltage.

Furthermore, since the WSe_2:Nb and WSe_2:Re forming the diode are heavily *p*- and *n*-type doped, even a small reverse bias (i.e. WSe_2:Nb is negatively biased with respect to WSe_2:Re) is able to shift the valence band maximum (VBM) of WSe_2:Nb above the conduction band minimum of WSe_2:Re (left panel of Fig. 3 (b)), enabling the direct tunneling of electrons from the valence band of WSe_2:Nb to the conduction band of WSe_2:Re. When under forward bias (i.e. WSe_2:Nb is positively biased with respect to WSe_2:Re), there are two current paths contributing to the total forward current: (I) tunneling-mediated interlayer recombination between majority carriers, and (II) thermionic emission of carriers over an energy barrier due to band offset, as shown in the right panel of Fig. 3(b). At relatively low forward bias voltages (< 1 V), the interlayer recombination current dominates the thermionic emission current due to the large band offset across the junction. As the forward bias voltage approaches about 1 V (corresponding to the band gap of WSe_2), the band offset and thus the energy barrier for the thermionic emission current diminishes, leading to a rapid increase of current. It is also worth pointing out that the ohmic contacts enabled by heavy *p*- and *n*-doping in our devices are crucial to the observation of intrinsic properties, such as the BTBT and backward diode behavior, of our van der Waals *p*-*n* tunnel junctions. Large parasitic resistance of the contacts was previously reported to severely limit both the reverse and forward currents in MoS_2/ WSe_2 van der Waals tunnel diodes [15]. Heavily doped TMDs can also be used to form low resistance Ohmic contacts to a wide range of two-dimensional semiconductors as recently demonstrated by the authors [9].

IV. CONCLUSIONS

In conclusion, we have synthesized both *p*- and *n*-type WSe_2 crystals with high carrier densities using Nb and Re as dopants, respectively. Electrical transport measurements performed on both bulk crystals and FET devices

consisting of multilayers of Nb- and Re-doped WSe_2 show that WSe_2:Nb is degenerately hole-doped, whereas electrons in WSe_2:Re are largely trapped in localized states. The availability of highly doped *n*-type and *p*-type WSe_2 enabled us to fabricate vertical van der Waals tunnel diodes that show reverse rectifying behavior, providing strong evidence of BTBT. The demonstration of BTBT is an important step toward the application of TMDs in a tunnel transistor.

V. ACKNOWLEDGMENTS

RM, MK, and DGM were supported by the Gordon and Betty Moore Foundation's EPiQS Initiative through Grant GBMF4416. H.C. and Z.Z. acknowledge partial support by NSF grant number DMR-1308436.

[1] G.-H. Lee, Y.-J. Yu, X. Cui, N. Petrone, C.-H. Lee, M. S. Choi, D.-Y. Lee, C. Lee, W. J. Yoo, K. Watanabe, and T. Taniguchi, Flexible and transparent MoS2 field-effect transistors on hexagonal boron nitride-graphene heterostructures, ACS Nano **7**, 7931 (2013).

[2] S. Das, R. Gulotty, A. V. Sumant, and A. Roelofs, All two-dimensional, flexible, transparent, and thinnest thin film transistor, Nano Letters **14**, 2861 (2014).

[3] H.-Y. Chang, S. Yang, J. Lee, L. Tao, W.-S. Hwang, D. Jena, N. Lu, and D. Akinwande, High-performance, highly bendable MoS2 transistors with high-k dielectrics for flexible low-power systems, ACS Nano **7**, 5446 (2013).

[4] Q. H. Wang, K. Kalantar-Zadeh, A. Kis, J. N. Coleman, and M. S. Strano, Electronics and optoelectronics of two-dimensional transition metal dichalcogenides, Nature Nanotechnology **7**, 699 (2012).

[5] V. Podzorov, M. Gershenson, C. Kloc, R. Zeis, and E. Bucher, High-mobility field-effect transistors based on transition metal dichalcogenides, Applied Physics Letters **84**, 3301 (2004).

[6] H. Fang, S. Chuang, T. C. Chang, K. Takei, T. Takahashi, and A. Javey, High-performance single layered WSe2 p-FETs with chemically doped contacts, Nano Letters **12**, 3788 (2012).

[7] H. Fang, M. Tosun, G. Seol, T. C. Chang, K. Takei, J. Guo, and A. Javey, Degenerate n-doping of few-layer transition metal dichalcogenides by potassium, Nano Letters **13**, 1991 (2013).

[8] W. Liu, J. Kang, D. Sarkar, Y. Khatami, D. Jena, and K. Banerjee, Role of metal contacts in designing high-performance monolayer n-type WSe2 field effect transistors, Nano Letters **13**, 1983 (2013).

[9] H.-J. Chuang, X. Tan, N. J. Ghimire, M. M. Perera, B. Chamlagain, M. M.-C. Cheng, J. Yan, D. Mandrus, D. Tomanek, and Z. Zhou, High mobility wse2 p-and n-type field-effect transistors contacted by highly doped graphene for low-resistance contacts, Nano Letters **14**, 3594 (2014).

[10] H. Fang, C. Battaglia, C. Carraro, S. Nemsak, B. Ozdol, J. S. Kang, H. A. Bechtel, S. B. Desai, F. Kronast, A. A. Unal, and G. Conti, Strong interlayer coupling in van der Waals heterostructures built from single-layer chalcogenides, Proceedings of the National Academy of Sciences **111**, 6198 (2014).

[11] C.-H. Lee, G.-H. Lee, A. M. van Der Zande, W. Chen, Y. Li, M. Han, X. Cui, G. Arefe, C. Nuckolls, T. F. Heinz, and J. Guo, Atomically thin p–n junctions with van der Waals heterointerfaces, Nature Nanotechnology (2014).

[12] M. M. Furchi, A. Pospischil, F. Libisch, J. BurgdoÌĹrfer, and T. Mueller, Photovoltaic effect in an electrically tunable van der Waals heterojunction, Nano Letters **14**, 4785 (2014).

[13] X. Hong, J. Kim, S.-F. Shi, Y. Zhang, C. Jin, Y. Sun, S. Tongay, J. Wu, Y. Zhang, and F. Wang, Ultrafast charge transfer in atomically thin MoS2/WS2 heterostructures, Nature Nanotechnology (2014).

[14] J. Suh, T.-E. Park, D.-Y. Lin, D. Fu, J. Park, H. J. Jung, Y. Chen, C. Ko, C. Jang, Y. Sun, and R. Sinclair, Doping against the native propensity of MoS2: degenerate hole doping by cation substitution, Nano Letters **14**, 6976 (2014).

[15] T. Roy, M. Tosun, X. Cao, H. Fang, D.-H. Lien, P. Zhao, Y.-Z. Chen, Y.-L. Chueh, J. Guo, and A. Javey, Dual-Gated MoS2/WSe2 van der Waals Tunnel Diodes and Transistors, ACS Nano **9**, 2071 (2015).

[16] Y. Du, H. Liu, A. T. Neal, M. Si, and P. D. Ye, Molecular Doping of Multilayer Field-Effect Transistors: Reduction in Sheet and Contact Resistances, Electron Device Letters, IEEE **34**, 1328 (2013).

[17] D. Kiriya, M. Tosun, P. Zhao, J. S. Kang, and A. Javey, Air-stable surface charge transfer doping of MoS2 by benzyl viologen, Journal of the American Chemical Society **136**, 7853 (2014).

[18] L. Yang, K. Majumdar, H. Liu, Y. Du, H. Wu, M. Hatzistergos, P. Hung, R. Tieckelmann, W. Tsai, C. Hobbs, and P. Ye, Chloride molecular doping technique on 2D materials: WS2 and MoS2, Nano Letters **14**, 6275 (2014).

[19] R. Fivaz and E. Mooser, Mobility of charge carriers in semiconducting layer structures, Physical Review **163**, 743 (1967).

[20] A. Klein, P. Dolatzoglou, M. Lux-Steiner, and E. Bucher, Structure and tribological properties of WSe x, WSe x/TiN, WSe x/TiCN and WSe x/TiSiN coatings, Solar energy materials and solar cells **46**, 175 (1997).

[21] M. R. Laskar, D. N. Nath, L. Ma, E. W. Lee II, C. H. Lee, T. Kent, Z. Yang, R. Mishra, M. A. Roldan, J.-C. Idrobo, and S. T. Pantelides, Possible doping strategies for MoS 2 monolayers: An ab initio study, Applied Physics Letters **104**, 092104 (2014).

[22] D. Shtansky, T. Lobova, V. Y. Fominski, S. Kulinich, I. Lyasotsky, M. Petrzhik, E. Levashov, and J. Moore, Electronic transport and device prospects of monolayer molybdenum disulphide grown by chemical vapour deposition, Surface and Coatings Technology **183**, 328 (2004).

[23] K. Dolui, I. Rungger, C. D. Pemmaraju, and S. Sanvito, Electronic properties of doped semiconductors, Physical Review B **88**, 075420 (2013).

[24] W. Zhu, T. Low, Y.-H. Lee, H. Wang, D. B. Farmer, J. Kong, F. Xia, and P. Avouris, Tunnel field-effect transistors as energy-efficient electronic switches, Nature Communications **5** (2014).

[25] B. I. Shklovskii and A. L. Efros, Two-dimensional to three-dimensional tunneling in InAs/AlSb/GaSb quantum well heterojunctions, Moscow Izdatel Nauka **1** (1979).

[26] H. Zhou, C. Wang, J. C. Shaw, R. Cheng, Y. Chen, X. Huang, Y. Liu, N. O. Weiss, Z. Lin, Y. Huang, and X. Duan, Large Area Growth and Electrical Properties of p-Type WSe2 Atomic Layers, Nano Letters **15**, 709 (2014).

[27] H. Fang, S. Chuang, T. C. Chang, K. Takei, T. Takahashi, and A. Javey, High-performance single layered WSe2 p-FETs with chemically doped contacts, Nano Letters **12**, 3788 (2012).

[28] W. Zhu, T. Low, Y.-H. Lee, H. Wang, D. B. Farmer, J. Kong, F. Xia, and P. Avouris, Electronic transport and device prospects of monolayer molybdenum disulphide grown by chemical vapour deposition, Nature Communications **5** (2014).

[29] B. W. Baugher, H. O. Churchill, Y. Yang, and P. Jarillo-Herrero, Intrinsic electronic transport properties of high-quality monolayer and bilayer MoS2, Nano Letters **13**, 4212 (2013).

[30] A. M. Ionescu and H. Riel, Influence of material synthesis and doping on the transport properties of WSe 2 single crystals grown by selenium transport, Nature **479**, 329 (2011).

[31] Y. Zeng, C.-I. Kuo, R. Kapadia, C.-Y. Hsu, A. Javey, and C. Hu, p-type doping of MoS2 thin films using Nb, Journal of Applied Physics **114**, 024502 (2013).